

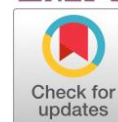
# The effect of silicon dioxide on the structural, thermal and transport properties of an organic ionic plastic crystal $(n\text{-C}_4\text{H}_9)_4\text{NBF}_4$

Ivan Stebnitskii <sup>ab\*</sup> , Yulia Mateyshina <sup>ab</sup> , Nikolai Uvarov <sup>ab</sup> 

**a:** Institute of Solid State Chemistry and Mechanochemistry, Siberian Branch of the Russian Academy of Sciences, Novosibirsk 630090, Russia

**b:** Department of Natural Sciences, Novosibirsk State University, Novosibirsk 630090, Russia

\* Corresponding author: [i.stebnitskii@g.nsu.ru](mailto:i.stebnitskii@g.nsu.ru)



This paper belongs to a Regular Issue.

## Abstract

Composite solid electrolytes based on an organic ionic plastic crystal  $(n\text{-C}_4\text{H}_9)_4\text{NBF}_4$  with highly dispersed  $\text{SiO}_2$  with specific surface area of  $S_s = 324 \pm 10 \text{ m}^2/\text{g}$  have been studied for the first time. By methods of X-ray diffraction and differential scanning calorimetry, it was found that the introduction of  $\text{SiO}_2$  leads to amorphization of the salt. An unusual size effect was observed in the composites: the temperature of the polymorphic transition of the salt shifted from  $67^\circ\text{C}$  to  $60^\circ\text{C}$ , while the melting point did not change. The  $0.15(n\text{-C}_4\text{H}_9)_4\text{NBF}_4\text{-}0.85\text{SiO}_2$  composite was found to possess the highest electrical conductivity ( $\sigma = 2 \cdot 10^{-5} \text{ S/cm}$  at  $150^\circ\text{C}$ ), which is 1.5 orders of magnitude higher than that of the initial salt. Modelling of the concentration dependences of the electrical conductivity of composites using the mixing equation showed that the reason for the increase in electrical conductivity is the formation of an amorphous layer of salt, the electrical conductivity of which is 3 orders of magnitude higher than that of the crystalline phase  $(n\text{-C}_4\text{H}_9)_4\text{NBF}_4$ . The obtained results can be used for the design of high-performance composites based on organic ionic plastic crystals for application in electrochemical devices.

## Keywords

solid composite electrolytes  
organic ionic plastic crystal  
ionic conductivity  
tetrabutylammonium tetrafluoroborate  
silicon dioxide

Received: 27.05.24

Revised: 25.06.24

Accepted: 15.07.24

Available online: 30.07.24

## Key findings

- Silicon dioxide with a high specific surface area leads to the amorphization of  $(n\text{-C}_4\text{H}_9)_4\text{NBF}_4$ .
- The best conductivity of  $2 \cdot 10^{-5} \text{ S/cm}$  at  $150^\circ\text{C}$  was observed for  $0.15(n\text{-C}_4\text{H}_9)_4\text{NBF}_4\text{-}0.85\text{SiO}_2$  composite.
- The increase in conductivity is caused by the formation of a highly conductive amorphous phase of the salt, the conductivity of which is 3 orders of magnitude higher than that of the crystalline salt.

© 2024, the Authors. This article is published in open access under the terms and conditions of the Creative Commons Attribution (CC BY) license (<http://creativecommons.org/licenses/by/4.0/>).

## 1. Introduction

For the development of electrochemical energy storage devices, researchers around the world are increasingly focusing on solid electrolytes as an alternative to traditional liquid electrolytes [1–3]. The use of such electrolytes will improve the mechanical properties and safety of the devices as well as simplify the assembly technology of electrochemical energy storage devices [4–6]. However, many solid electrolytes are characterized by poor contact with electrodes, are unstable in air and have low ionic conductivity compared to liquid electrolytes [7, 8]. In this regard, the

search for promising solid electrolytes and the improvement of the physico-chemical properties of already known ones are actively carried out.

Organic ionic plastic crystals (OIPCs) represent an interesting class of materials including salts of tetraalkylammonium [9], pyrrolidinium [10, 11], imidazolium [12], tetraalkylphosphonium [13], morpholinium [14] with a wide variety of anions, including quite non-trivial ones, such as bis(trifluoromethanesulfonyl)imide (TFSI) [15] and carbamoylcyano(nitroso)methanide [16]. A common feature of OIPCs is high thermal and electrochemical stability, plasticity, and rather high ionic conductivity due to local orientational or rotational disorder of ions or

their parts [17,18]. For example, diethyl(methyl)(isobutyl)phosphonium hexafluorophosphate provides an electrical conductivity of  $10^{-3}$  S/cm at 120 °C in the solid phase at the highest temperatures [19]. However, in most cases, OIPCs exhibit rather low electrical conductivity,  $\sigma \approx 10^{-5} - 10^{-6}$  S/cm, near the melting point [20,21].

A promising way to improve the transport properties of ionic compounds is to create composites with inert additives. By choosing appropriate heterogeneous additive, it is possible to control the physico-chemical properties of composites, in particular to, improve transport properties. Previously, heterogeneous doping has been extensively studied for inorganic systems, and the main regularities have been revealed. A number of works have demonstrated that the introduction of oxides leads to a significant increase in electrical conductivity by several orders of magnitude [22–24]. It is known that the electrical conductivity of composites increases with decreasing oxide particle size (which is approximately equivalent to an increase in specific surface area) [25]. In early studies it was also found that the absolute value of conductivity is influenced by the chemical nature of the oxide. Thus, in most cases, the best conductivity values were achieved when using basic oxides as additives, in particular, in  $\text{LiClO}_4 - \text{A}$  composites ( $\text{A} = \text{MgO}$  [26],  $\text{Al}_2\text{O}_3$  [27],  $\text{SiO}_2$  [27]), the maximum conductivity was observed when  $\text{MgO}$  was used. However, in some systems, on the contrary, the best effect were observed when acidic oxides were used: for example, in the  $\text{CsNO}_2 - \text{A}$  systems ( $\text{A} = \text{MgO}$ ,  $\text{Al}_2\text{O}_3$ ,  $\text{SnO}_2$  [28]), the maximum conductivity values were observed when acidic oxide was used as an additive. Thus, it is rather unclear how the chemical nature of the oxide affects the transport properties in a particular class of substances.

Previously, composites based on OIPCs were studied in different scientific groups [29–31]. It has been shown that the introduction of nanosized inert additives of different chemical nature leads to a significant increase in the conductivity of salts. However, at the moment there are almost no systematic studies of composites based on OIPCs.

Earlier we have studied the composites based on one of the OIPC representatives – tetrabutylammonium tetrafluoroborate – with various nanosized inert additives ( $\text{MgO}$  [32],  $\text{Al}_2\text{O}_3$  [29], nanodiamonds [33]), but composites with acidic oxides remain unexplored. In this work, we investigated the effect of the addition of acidic oxide  $\text{SiO}_2$ , characterized by high specific surface area, on the structural, thermal and transport properties of  $(n\text{-C}_4\text{H}_9)_4\text{NBF}_4$  in comparison with previously used heterogeneous additives.

## 2. Materials and methods

### 2.1. Materials

Tetra-*n*-butylammonium tetrafluoroborate  $(n\text{-C}_4\text{H}_9)_4\text{NBF}_4$  (hereafter  $\text{Bu}_4\text{NBF}_4$ ) was synthesized by an exchange reaction between  $(n\text{-C}_4\text{H}_9)_4\text{NBr}$  (Sigma Aldrich, reagent grade) and an aqueous solution of  $\text{HBF}_4$  (Sigma Adrich, 48 mas.%).

The resulting white precipitate was filtered, then recrystallized from an aqueous-alcohol solution and dried at 120 °C. As a silicon dioxide  $\text{SiO}_2$  additive, a mesoporous silica gel of the KSM grade (JSC “SKTB Katalizator”, Russia, 99% pure, specific surface area  $S_{\text{sp}} = 324 \pm 10$  m<sup>2</sup>/g, specific pore volume 0.193 cm<sup>3</sup>/g, average pore size 2.392 nm) was used. Before use,  $\text{SiO}_2$  was calcined at 500 °C for several hours to remove adsorbed water molecules. Composites  $(1-x)\text{Bu}_4\text{NBF}_4-x\text{SiO}_2$  ( $0 \leq x < 1$ ,  $x$  – molar fraction) were prepared by mixing stoichiometric quantities of initial compounds with the addition of a small amount of ethanol in an agate mortar. The resulting mixtures were then heated in a drying oven at 150 °C for one hour to remove any remaining solvent. In order to ensure a uniform distribution of particles throughout the composites, this process was repeated three times.

### 2.2. Methods

To investigate the phase composition of the composites, the X-ray diffraction was carried out on D8 Advance diffractometer (Bruker, Germany) using  $\text{Cu K}\alpha$  radiation, with  $\text{K}\beta$  filter and one-dimensional Lynx-Eye detector over the angle range of  $5^\circ < 2\theta < 90^\circ$  with the angle step of  $\Delta 2\theta = 0.0195^\circ$ . Thermal properties were studied using a differential scanning calorimeter DSC-500 (Sam STU, Russia). For experiments, 5–10 mg of the powder sample was placed in a closed aluminum crucible and heated from 20 to 200 °C in an argon atmosphere at a rate of 10 °C/min. IR absorption spectra were measured on Vector 22 by the attenuated total reflectance (ATR) method. The transport properties were studied by impedance spectroscopy in a two-electrode mode on a Hewlett Packard HP 4284 A Precision LCR Meter (Hewlett-Packard, Japan) in a low-vacuum ( $5 \cdot 10^{-2}$  Torr) in the frequency range 30 Hz – 1 MHz. For measurements, the sample powders were compacted into pellets with a diameter of 6.2–6.3 mm and a thickness of 0.5–1.5 mm with silver powder electrodes at a pressure of 100 MPa. The resistance of the samples,  $R$ , at each temperature was calculated from the analysis of the Nyquist complex impedance plots  $Z^* = Z' - iZ''$  by fitting the theoretical values calculated for the model equivalent circuits to the experimental ones using the Zview software (version 3.1, Scribner Associates, Inc., USA). The total conductivity was calculated using the ratio  $\sigma = h/(R \cdot S)$ , where  $h$  and  $S$  are the thickness and electrode area of the pellet, respectively.

## 3. Results and Discussion

### 3.1. X-ray diffraction studies

The phase composition of  $(1-x)\text{Bu}_4\text{NBF}_4-x\text{SiO}_2$  composites was studied by X-ray diffraction; the results are shown in Figure 1. In the diffraction patterns, only the reflections of the stable at room temperature low-temperature  $\text{Bu}_4\text{NBF}_4$  phase (space group  $\text{P}2_1/\text{c}$ , according to our previous studies [33]) are present. Reflections of  $\text{SiO}_2$  were not observed due to its amorphous structure.

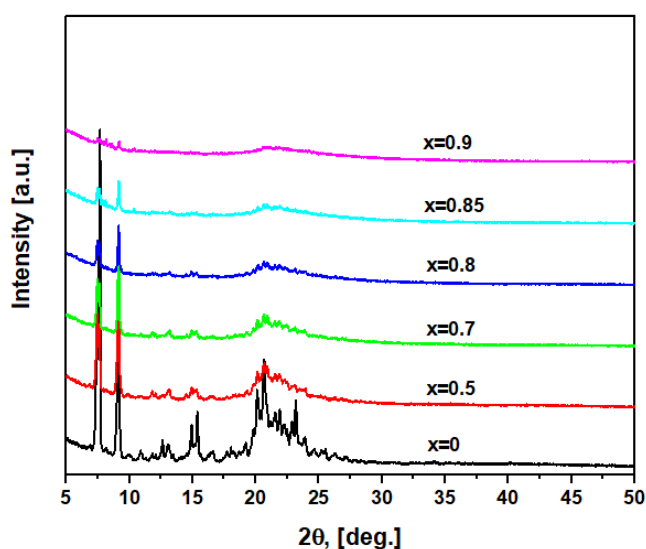


**Figure 1** X-ray diffraction patterns of composites  $(1-x)$   $\text{Bu}_4\text{NBF}_4-x\text{SiO}_2$ , recorded at ambient temperature.

With an increase in the molar fraction of  $\text{SiO}_2$ , a sharp decrease in the intensity of salt reflections was observed: for example, at  $x = 0.9$  the intensity of the peak observed at  $2\theta = 9.12^\circ$  decreases by 7 times, while the salt content in the composite was 42.8 vol.%. This effect can be explained by a partial amorphization of the salt in the composite.

### 3.2. Thermal properties

According to the literature data, the initial  $\text{Bu}_4\text{NBF}_4$  is characterized by the presence of several phase transitions: polymorphic transition at 62–67 °C and melting at 159–161 °C (the temperature variation is due to different heating rates) [9, 13]. In addition, after fast cooling of the salt from the melt to room temperature, a metastable phase forms, which undergoes a phase transition to a high-temperature phase at 41 °C [33].

The thermal properties of the composites were studied by differential scanning calorimetry (DSC). In the DSC curves obtained upon heating, two phase transitions are ob-

served, associated with the polymorphic transition: polymorphic transition (60–62 °C) and melting of  $\text{Bu}_4\text{NBF}_4$  (163–164 °C) (Figure 2), respectively. The decrease of the polymorphic transition temperature from 67 °C to 60–62 °C is noteworthy. Most probably, this effect is due to the size effect as in earlier studies [34]. At the same time, it is quite unusual that along with the shift in the polymorphic transition temperature, there is no size effect during salt melting.

With increasing molar fraction of  $\text{SiO}_2$  in composites, a sharp decrease in enthalpy of phase transitions of salts is observed. At high concentrations of  $\text{SiO}_2$ , phase transitions completely disappear. Previously, a similar effect was observed in other composites of the "ionic salt-oxide" type, such as  $\text{LiClO}_4 - \text{MgO}$  [26],  $\text{RbNO}_3 - \text{Al}_2\text{O}_3$  [35],  $(n\text{-C}_4\text{H}_9)_3\text{CH}_3\text{NBF}_4 - \text{nanodiamonds}$  [36]. A similar phenomenon is associated with the salt amorphization near the salt-oxide phase contact.

As the amorphization of the salt occurs in the interfaces, the highest effect will be achieved at the maximal number of salt|additive contacts. Heterogeneous additives may differ in molar mass and density; therefore, in order to correctly compare the effect of different additives, it is necessary to consider the relative change in enthalpy, expressed in  $\text{J}/\text{cm}^3$ , and the volume fraction of the additive. For conversion of the molar fraction of  $\text{SiO}_2$   $x$  into the volume fraction  $f$  the following equation may be used:

$$f = \frac{x}{x + (1-x) \cdot \frac{M_1 \cdot \rho_2}{M_2 \cdot \rho_1}}, \quad (1)$$

where  $M_1$  and  $M_2$  are the molar mass of salt and  $\text{SiO}_2$ , respectively,  $\rho_1 = 1.0 \text{ g}/\text{cm}^3$  and  $\rho_2 = 2.2 \text{ g}/\text{cm}^3$  are the density of salt and  $\text{SiO}_2$ . The experimental values of the relative enthalpy of melting differ significantly from those in the case of a random mixture of components without interfacial interaction (Figure 3). It is worth noting that although  $\text{SiO}_2$  has an effect on the amorphization of  $(n\text{-C}_4\text{H}_9)_4\text{NBF}_4$ , the effect of other additives, such as nanodiamonds [31], is more pronounced.

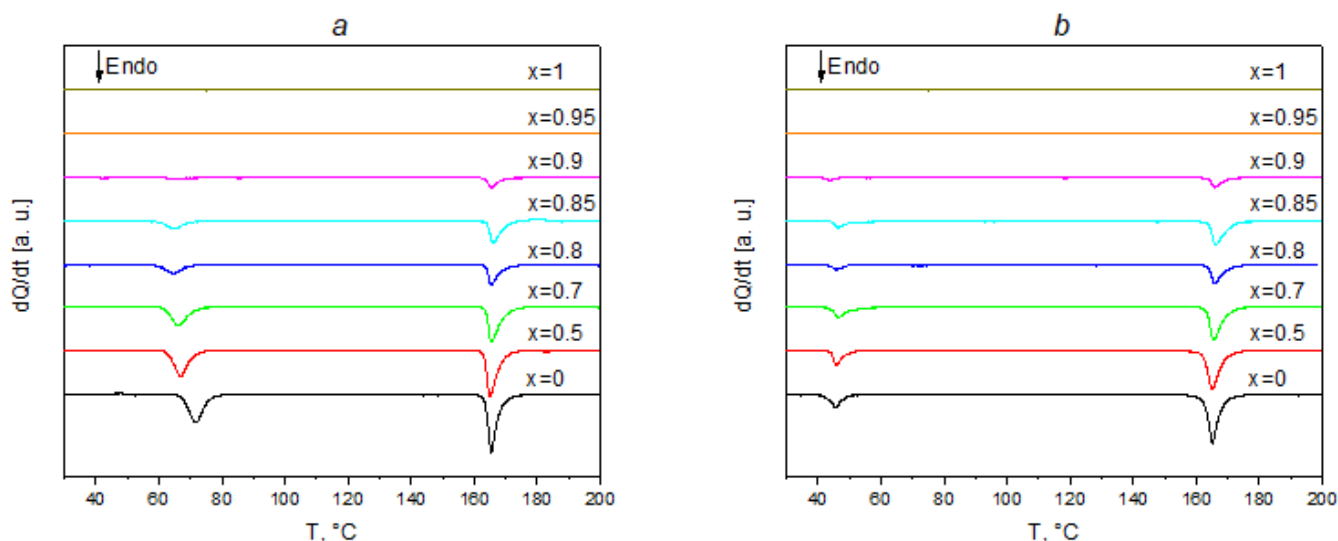


**Figure 2** DSC curves for  $(1-x)$   $\text{Bu}_4\text{NBF}_4 - x\text{SiO}_2$  composites on first (a) and second (b) heating.

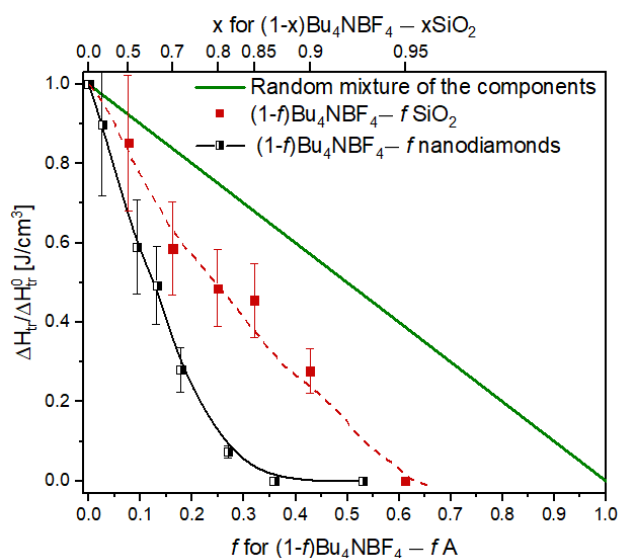


**Figure 3** Experimental values of relative melting enthalpy of  $\text{Bu}_4\text{NBF}_4$  in  $(1-f)\text{Bu}_4\text{NBF}_4 - fA$  (where  $A = \text{SiO}_2$  [this work] and nanodiamonds [33]) in comparison with the dependence expected for random mixture of components (line). The upper axis shows the molar fractions of  $\text{SiO}_2$  in  $(1-x)\text{Bu}_4\text{NBF}_4 - x\text{SiO}_2$  composites.

### 3.3. IR spectroscopy study

The IR spectroscopy method was used to study the effect of  $\text{SiO}_2$  on the local environment of atoms in  $\text{Bu}_4\text{NBF}_4$ . Vibrations in the  $\text{BF}_4^-$  ion were used as a probe to determine the processes occurring in the system  $(1-x)\text{Bu}_4\text{NBF}_4 - x\text{SiO}_2$ . According to the literature data, the  $\text{BF}_4^-$  ion is characterized by four vibrations: totally symmetric stretching  $\nu_1(A_1) \sim 770\text{ cm}^{-1}$ , deformation  $\nu_3(E) \sim 360\text{ cm}^{-1}$ , antisymmetric stretching  $\nu_3(F_2) \sim 1100\text{ cm}^{-1}$  and deformation vibrations  $\nu_4(F_1) \sim 520\text{ cm}^{-1}$  [29, 37]. Only the last two are allowed in the IR spectra.

Figure 4 shows the IR spectra of  $(1-x)\text{Bu}_4\text{NBF}_4 - x\text{SiO}_2$ . The resulting spectra are the sum of the spectra of individual components. With an increase in the proportion of  $\text{SiO}_2$ , the intensities of all bands decrease slightly. It was previously shown that the disordering of  $\text{Bu}_4\text{NBF}_4$  leads to a decrease in the symmetry of the  $\text{BF}_4^-$  anion, which leads to the appearance of the forbidden mode  $\nu_1(A_1)$  [29]. In pure  $\text{Bu}_4\text{NBF}_4$ , a low-intensity peak is observed at  $800\text{ cm}^{-1}$ , which can be attributed to the forbidden mode  $\nu_1(A_1)$ , while with

increasing  $x$  a shift of this peak from  $800\text{ cm}^{-1}$  to  $789\text{ cm}^{-1}$  is observed. Thus, during the transition from pure salt to composite, the structure of  $\text{Bu}_4\text{NBF}_4$  becomes disordered.

### 3.4. Transport properties

The transport properties of the composites were studied by impedance spectroscopy. At each temperature point, an impedance hodograph was recorded, the typical form of which in Nyquist coordinates is shown in Figure 5. The hodographs were described by an equivalent electrical circuit consisting of three impedances connected in series: the bulk impedance  $Z_{\text{bulk}}$ , which includes a parallel-connected resistance  $R_{\text{bulk}}$  and a constant-phase element  $\text{CPE}_{\text{bulk}}$ , the impedance  $Z_{\text{surface}}$ , consisting of a parallel-connected resistance  $R_{\text{surface}}$  and a constant-phase element  $\text{CPE}_{\text{surface}}$ , as well as an electrode impedance described by a constant-phase element  $\text{CPE}_{\text{el}}$ . The impedance  $Z_{\text{bulk}}$  describes the resistance of the bulk phase of the salt; the impedance  $Z_{\text{surface}}$  describes the resistance of the salt located in the  $\text{SiO}_2$  pores.

Figure 6a shows the temperature dependence of the conductivity of  $(1-x)\text{Bu}_4\text{NBF}_4 - x\text{SiO}_2$  composites. The conductivity of composites increased monotonously with temperature and was reproduced in heating-cooling cycles, which indicates the absence of influence of water adsorbed on the oxide surface on the conductivity values.

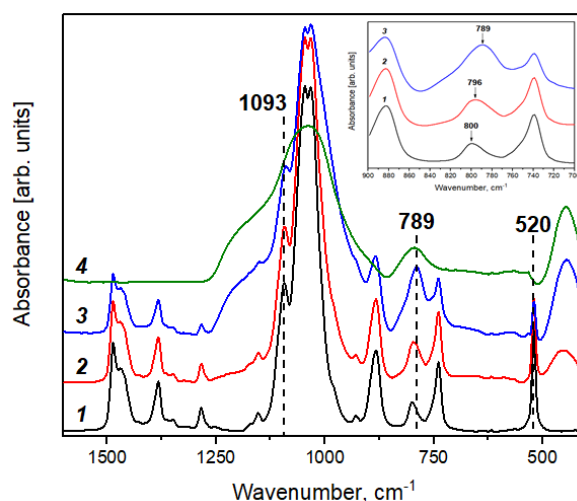


**Figure 4** IR-spectra of pure  $\text{Bu}_4\text{NBF}_4$  (1),  $0.5\text{Bu}_4\text{NBF}_4 - 0.5\text{SiO}_2$  (2),  $0.15\text{Bu}_4\text{NBF}_4 - 0.85\text{SiO}_2$  (3) and pure  $\text{SiO}_2$  (4) recorded at room temperature. The inset shows the area  $700\text{--}900\text{ cm}^{-1}$ .

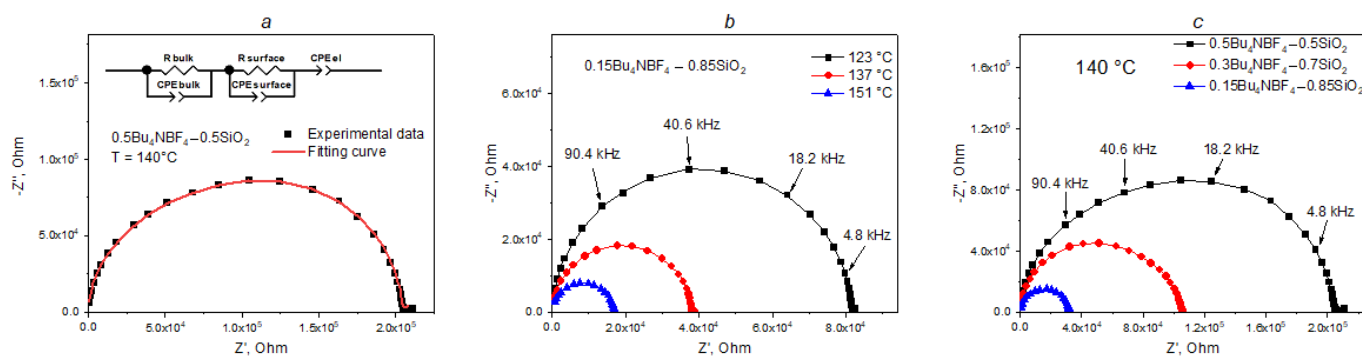


**Figure 5** Typical complex impedance plots:  $0.5\text{Bu}_4\text{NBF}_4 - 0.5\text{SiO}_2$  at  $140\text{ }^\circ\text{C}$  (a);  $0.15\text{Bu}_4\text{NBF}_4 - 0.85\text{SiO}_2$  at  $123\text{ }^\circ\text{C}$ ,  $137\text{ }^\circ\text{C}$  and  $151\text{ }^\circ\text{C}$  (b);  $(1-x)\text{Bu}_4\text{NBF}_4 - x\text{SiO}_2$  ( $x = 0.5, 0.7, 0.85$ ) (c). The inset in Figure 5a shows the equivalent electrical circuit used for the simulation.



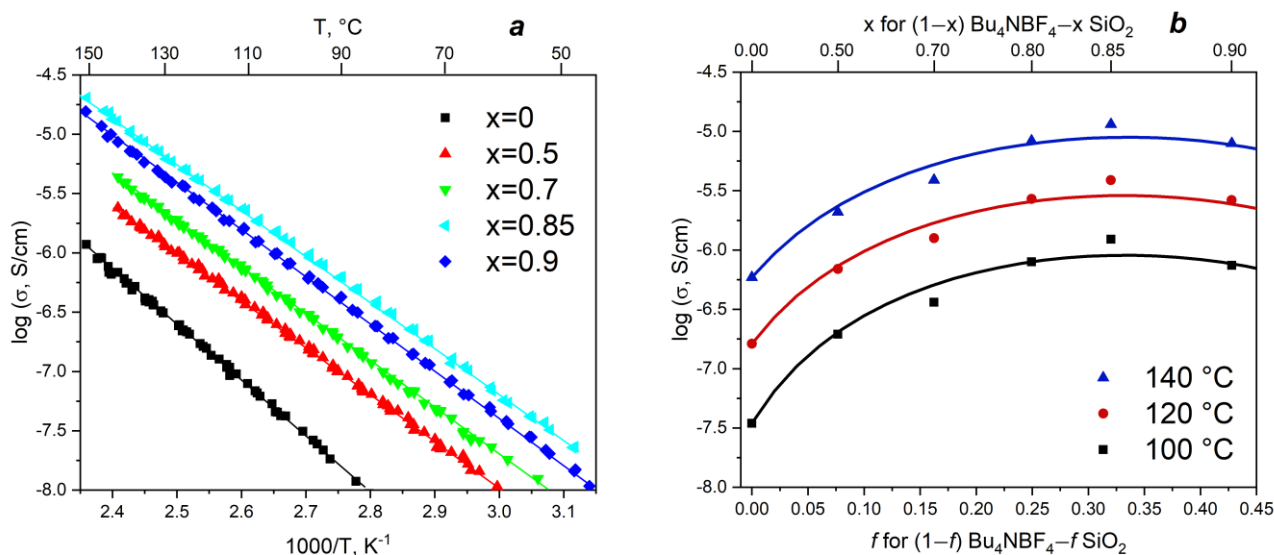


**Figure 6** Dependences of the conductivity of composites  $(1-x) \text{Bu}_4\text{NBF}_4-x\text{SiO}_2$  from: the reciprocal temperature (a); the volume fraction  $f$  and molar fraction  $x$  of  $\text{SiO}_2$  at temperatures of 100, 120 and 140 °C (b).

The presented dependences obey the Arrhenius equation  $\sigma \cdot T = A \cdot \exp(-E_a/RT)$  ( $A$  is the pre-exponential factor,  $E_a$  is the activation energy of conductivity) throughout the studied range of  $\text{SiO}_2$  concentrations. The introduction of  $\text{SiO}_2$  leads to a slight decrease in the activation energy of the conductivity, while the  $E_a$  values within the measurement accuracy are the same for all compositions (Table 1). Compared to a pure  $\text{Bu}_4\text{NBF}_4$ , in the composites the values of the pre-exponential factor decrease and then increase with increasing  $\text{SiO}_2$  concentration (Table 1).

It is known that in composites of the «ionic salt – oxide» type the excess conductivity is caused by ionic transport along interfaces. The maximum electrical conductivity is exhibited at the highest number of interfaces, which is usually observed at a volume ratio of the components close to 1:1. In this regard, it is more correct to analyze the dependences of conductivity on the volume fraction of the oxide.

Figure 6b shows the concentration dependence of the composites  $(1-x) \text{Bu}_4\text{NBF}_4-x\text{SiO}_2$  on the oxide volume fraction  $f$  (bottom) and mole fraction  $x$  (top). The conductivity of the composites may be qualitatively described by percolation model with two percolation thresholds. At low fractions of the additive the total conductivity is provided mainly by the bulk contribution of  $\text{Bu}_4\text{NBF}_4$ . At the first percolation threshold the contribution of the interface conductivity increases up to maximum values where this contribution dominates. With further increase in the oxide additive content near the second percolation, conductivity decreases due to the destruction of the interconnected network of highly conductive interface regions. Actually, percolation thresholds may be strongly diffused, hindering the application of the percolation model.

The percolation-like conductivity behavior of such composites can be described within the framework of the mixing model proposed by Uvarov [38]. Within the framework of this model, it is assumed that the experimental values of

the electrical conductivity of the composites are described by three contributions: the contribution of the crystalline phase of the salt  $\sigma_{\text{bulk}}$ , silicon oxide  $\sigma_2$  and the highly conductive regions of the salt  $\sigma_s$  (equation 2):

$$\sigma^{\alpha(f)} = \sigma_{\text{bulk}}^{\alpha(f)} \cdot (1 - f - f_s) + \sigma_s^{\alpha(f)} \cdot f_s + \sigma_2^{\alpha(f)} \cdot f \quad (2)$$

where  $f$  and  $f_s$  are the volume fraction of  $\text{SiO}_2$  and the interface amorphous phase of the salt, respectively. The  $f_s$  values were calculated from the dependence of the relative enthalpy of melting on  $f$  according to equation 3:

$$f_s = \beta \cdot \frac{\lambda}{L} \cdot f \cdot (1 - f), \quad (f_s \leq 1 - f), \quad (3)$$

where  $\beta$  is the geometric factor,  $\lambda$  is the thickness of the amorphous interface layer, and  $L$  is the average size of  $\text{SiO}_2$  crystallites. The coefficient  $\alpha(f)$  takes into account the morphology of the composite. In the simplest case,  $\alpha(f)$  is approximated by a linear function:

$$\alpha(f) = \alpha_1 \cdot (1 - f) + \alpha_2 \cdot f, \quad (4)$$

where  $\alpha_1$  and  $\alpha_2$  are the coefficients determined by the morphology of the composite in limiting cases.

As seen from Figure 6b, the mixing equation fairly describes the experimental data. The modelling results confirm the qualitative explanation of the variation in conductivity with the composition described above.

**Table 1** Experimental conductivity parameters for composites  $(1-x) \text{Bu}_4\text{NBF}_4-x\text{SiO}_2$ .

$x \text{ SiO}_2$	$E_a$ , (eV)	$\log A$ ( $\text{S} \cdot \text{K} \cdot \text{cm}^{-1}$ )
0	$0.95 \pm 0.01$	$8.0 \pm 0.1$
0.5	$0.82 \pm 0.01$	$6.92 \pm 0.03$
0.7	$0.82 \pm 0.01$	$7.14 \pm 0.03$
0.8	$0.80 \pm 0.01$	$7.23 \pm 0.03$
0.85	$0.80 \pm 0.01$	$7.43 \pm 0.03$
0.9	$0.81 \pm 0.01$	$7.41 \pm 0.03$

Estimation shows that the electrical conductivity of the amorphous phase is 3 orders of magnitude greater than that for the crystalline phase of the salt (Table 2).

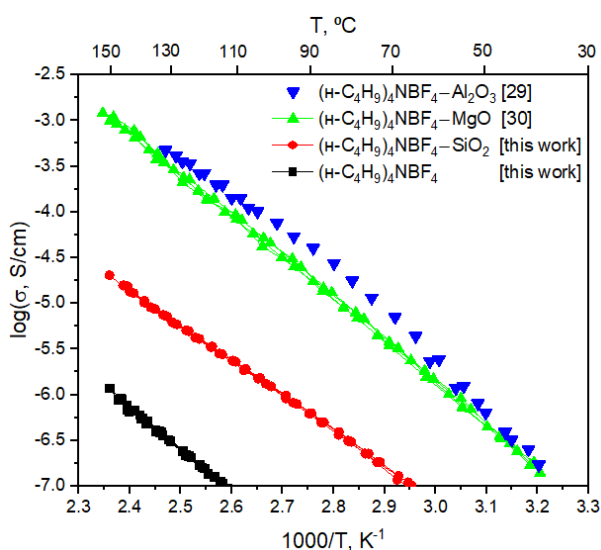
The fraction of amorphous phase of the salt increases with  $x$  or  $f$ , so at high concentrations of  $\text{SiO}_2$  the contribution of the interface conductivity of the salt becomes dominant. The maximum conductivity value of  $2 \cdot 10^{-5}$  S/cm is observed at  $150^\circ\text{C}$  for the composition  $x = 0.85$ , which corresponds to the volume fraction of the additive  $f = 32\%$ . Previously, a similar effect of increased conductivity was observed in other the ionic salt-oxide type composite electrolytes [26, 35]. The conductivity increase is attributed to the contribution of the highly-conducting amorphous interface phase of the salt formed as a result of the interface interaction between  $\text{SiO}_2$  and  $\text{Bu}_4\text{NBF}_4$ .

Figure 7 shows a comparison of temperature dependences of conductivity for  $\text{Bu}_4\text{NBF}_4$ -based composites with various oxides. The conductivity of  $\text{Bu}_4\text{NBF}_4$ -oxide composites strongly depends on both the specific surface area, concentration of the dopant and the chemical nature of the heterogeneous additive. For the comparison only oxide additives with specific surface area of  $200\text{--}300\text{ m}^2/\text{g}$  and the compositions corresponding to the highest conductivity value were selected.

It is seen that the introduction of any heterogeneous oxide additive into the dielectric salt  $\text{Bu}_4\text{NBF}_4$  leads to an increase in its conductivity by 1–3 orders of magnitude over the entire temperature range. There is a clear tendency: conductivity increases with basicity of the oxide additive in a series  $\text{SiO}_2\text{--Al}_2\text{O}_3\text{--MgO}$ .

**Table 2** Conductivity parameters obtained from the mixing equation.

Parameter	100 °C	120 °C	140 °C
$\sigma_{\text{bulk}}$ (S/cm)	$3.5 \cdot 10^{-8}$	$1.6 \cdot 10^{-7}$	$5.9 \cdot 10^{-7}$
$\sigma_s$ (S/cm)	$3.8 \cdot 10^{-5}$	$1.2 \cdot 10^{-4}$	$3.5 \cdot 10^{-4}$
$\alpha_1$		$0.29 \pm 0.01$	
$\alpha_2$		$0.09 \pm 0.02$	
$\beta \cdot \lambda / L$		$1.6 \pm 0.1$	



**Figure 7** A comparison of the conductivities of  $\text{Bu}_4\text{NBF}_4$  oxide composites.

## 4. Limitations

One of the limitations is the difficulty of indexing salt reflections in the X-ray diffraction patterns. At the moment, there are no crystallographic data on the  $(n\text{-C}_4\text{H}_9)_4\text{NBF}_4$  phase that is stable at room temperature in the databases. Structural analysis of the crystals of this salt is complicated by a number of factors: the low quality of the grown single crystals, disordered structure and the presence of only light atoms in the substance. In this regard, it is not possible to decipher the structure of  $(n\text{-C}_4\text{H}_9)_4\text{NBF}_4$  from single-crystal X-ray diffraction data, and as a consequence, it is not possible to index the reflections. It is known that in some cases phase indexing can be carried out using powder X-ray diffraction data, but correct analysis requires the presence of well-separated reflections with high intensity. In our case, a large number of difficult to separate reflections with low intensity are observed. Thus, X-ray powder diffraction cannot help in phase indexing either.

Another limitation is that the mechanism of interaction of the components of the system, which leads to the formation of a highly conductive composite, remains unclear.

## 5. Conclusions

In this work, the properties of the composites based on  $(n\text{-C}_4\text{H}_9)_4\text{NBF}_4$  and highly dispersed  $\text{SiO}_2$  ( $S_{\text{sp}} = 324 \pm 10\text{ m}^2/\text{g}$ ) were studied for the first time. The addition of  $\text{SiO}_2$  does not lead to the formation of new bulk phases, while it contributes to the amorphization of the salt. The conductivity of the composites under study increases with the  $\text{SiO}_2$  concentration, reaching a maximum of  $0.02\text{ mS}/\text{cm}$  at  $150^\circ\text{C}$  for the composite  $0.15(n\text{-C}_4\text{H}_9)_4\text{NBF}_4\text{--}0.85\text{SiO}_2$ , which is 1.5 orders of magnitude higher than for pure salt. The concentration dependences of conductivity are well described using the general mixing equation. Modelling using the mixing equation shows that the interface amorphous phase of the salt gives the main contribution to the overall conductivity. The conductivity of this phase is 3 orders of magnitude higher than that in the bulk crystalline phase of  $(n\text{-C}_4\text{H}_9)_4\text{NBF}_4$ . It has also been shown that the addition of  $\text{SiO}_2$  causes much less conductivity enhancement effect compared to the nanocrystalline alumina or magnesia. Nevertheless, the results obtained may be useful for further development of highly conductive solid electrolytes based on organic ionic plastic crystals.

## • Supplementary materials

No supplementary materials are available.

## Funding

This work was supported by the Russian Science Foundation (project 20-13-00302), <https://www.rscf.ru/en>.

## ● Acknowledgments

None.

## ● Author contributions

Conceptualization: I.S., Y.M., N.U.

Data curation: Y.M.

Formal Analysis: I.S., Y.M.

Funding acquisition: N.U.

Investigation: I.S.

Methodology: I.S., Y.M.

Project administration: N.U.

Resources: N.U.

Supervision: N.U.

Validation: Y.M., N.U.

Visualization: I.S.

Writing – original draft: I.S.

Writing – review & editing: Y.M., N.U.

## ● Conflict of interest

The authors declare no conflict of interest.

## ● Additional information

Author IDs:

Ivan Stebnitskii, Scopus ID [58488613400](#);

Yulia Mateyshina, Scopus ID [6506782050](#);

Nikolai Uvarov, Scopus ID [7006949152](#).

Websites:

Institute of Solid State Chemistry and Mechanochemistry, <http://www.solid.nsc.ru/en/institute/general/>;

Novosibirsk State University, <https://english.nsu.ru/>.

## References

- Campanella D, Belanger D, Paoletta A. Beyond Garnets, Phosphates and Phosphosulfides Solid Electrolytes: New Ceramic Perspectives for All Solid Lithium Metal Batteries. *J Power Sources*. 2021;482:228949. doi:[10.1016/j.jpowsour.2020.228949](#)
- Li S, Zhang S, Shen L, Liu Q, Ma J, Lv W, He Y, Yang Q. Progress and Perspective of Ceramic/Polymer Composite Solid Electrolytes for Lithium Batteries. *Adv Sci*. 2020;7(5):1903088. doi:[10.1002/advs.20190308](#)
- Park KH, Bai Q, Kim DH, Oh DY, Zhu Y, Mo Y, Jung YS. Design Strategies, Practical Considerations, and New Solution Processes of Sulfide Solid Electrolytes for All-Solid-State Batteries. *Adv. Energy Mater*. 2018;8(18):1800035. doi:[10.1002/aenm.201800035](#).
- Ye T, Li L, Zhang Y. Recent Progress in Solid Electrolytes for Energy Storage Devices. *Adv. Funct. Mater*. 2020;30(29):2000077. doi:[10.1002/adfm.202000077](#).
- Kumaravel V, Bartlett J, Pillai SC. Solid Electrolytes for High-Temperature Stable Batteries and Supercapacitors. *Adv Energy Mater*. 2021;11(3):2002869. doi:[10.1002/aenm.202002869](#)
- Chen S, Wen K, Fan J, Bando Y, Golberg D. Progress and Future Prospects of High-Voltage and High-Safety Electrolytes in Advanced Lithium Batteries: From Liquid to Solid Electrolytes. *J. Mater. Chem. A*. 2018;6(25):11631–11663. doi:[10.1039/C8TA03358G](#)
- Hou M, Liang F, Chen K, Dai Y, Xue D. Challenges and Perspectives of NASICON-Type Solid Electrolytes for All-Solid-State Lithium Batteries. *Nanotechnol*. 2020;31(13):132003. doi:[10.1088/1361-6528/ab5be7](#)
- Wu Z, Xie Z, Yoshida A, Wang Z, Hao X, Abudula A, Guan G. Utmost Limits of Various Solid Electrolytes in All-Solid-State Lithium Batteries: A Critical Review. *Renew Sustain Energy Rev*. 2019;109:367–385. doi:[10.1016/j.rser.2019.04.035](#)
- Uvarov NF, Iskakova AA, Bulina NV, Gerasimov KB, Slobodyuk AB, Kavun VYa. Ion Conductivity of the Plastic Phase of the Organic Salt [(C<sub>4</sub>H<sub>9</sub>)<sub>4</sub>N]BF<sub>4</sub>. *Russ J Electrochem*. 2015;51(5):491–494. doi:[10.1134/S102319351505016X](#)
- Abeysooriya S, Makhlooghiyaz F, Chotard J-N, O'Dell LA, Pringle JM. Investigation of the Physicochemical Properties of Pyrrolidinium-Based Mixed Plastic Crystal Electrolytes. *J Phys Chem C*. 2023;127(25):12304–12320. doi:[10.1021/acs.jpcc.3c02249](#)
- Pringle JM, Adebahr J, MacFarlane DR, Forsyth M. Unusual Phase Behaviour of the Organic Ionic Plastic Crystal N,N-Dimethylpyrrolidinium Tetrafluoroborate. *Phys Chem Chem Phys*. 2010;12(26):7234–7240. doi:[10.1039/B925501J](#)
- Chae H, Lee Y-H, Yang M, Yoon W-J, Yoon DK, Jeong K-U, Song YH, Choi UH, Lee M. Interesting Phase Behaviors and Ion-Conducting Properties of Dicationic N -Alkylimidazolium Tetrafluoroborate Salts. *RSC Adv*. 2019;9(7):3972–3978. doi:[10.1039/C8RA09208G](#)
- Matsumoto K, Harinaga U, Tanaka R, Koyama A, Hagiwara R, Tsunashima K. The Structural Classification of the Highly Disordered Crystal Phases of [Nn][BF<sub>4</sub>], [Nn][PF<sub>6</sub>], [Pn][BF<sub>4</sub>], and [Pn][PF<sub>6</sub>] Salts (Nn+ = Tetraalkylammonium and Pn+ = Tetraalkylphosphonium). *Phys. Chem. Chem. Phys*. 2014;16(43):23616–23626. doi:[10.1039/C4CP03391D](#)
- Sourjah A, Kang CSM, Doherty CM, Acharya D, O'Dell LA, Pringle JM. New Organic Ionic Plastic Crystals Utilizing the Morpholinium Cation. *Phys Chem Chem Phys*. 2023;25(24):16469–16482. doi:[10.1039/D3CP00759F](#)
- MacFarlane DR, Meakin P, Sun J, Amini N, Forsyth M. Pyrrolidinium Imides: A New Family of Molten Salts and Conductive Plastic Crystal Phases. *J Phys Chem. B*. 1999;103(20):4164–4170. doi:[10.1021/jp984145s](#)
- Janikowski J, Razali MR, Forsyth CM, Nairn KM, Batten SR, MacFarlane DR, Pringle JM. Physical Properties and Structural Characterization of Ionic Liquids and Solid Electrolytes Utilizing the Carbamoylcyanonitrosomethanide Anion. *ChemPlusChem*. 2013;78(6):486–497. doi:[10.1002/cplu.201300068](#)
- Zhu H, MacFarlane DR, Pringle JM, Forsyth M. Organic Ionic Plastic Crystals as Solid-State Electrolytes. *Trends Chem*. 2019;1(1):126–140. doi:[10.1016/j.trechm.2019.01.002](#)
- Pringle JM, Howlett PC, MacFarlane DR, Forsyth M. Organic Ionic Plastic Crystals: Recent Advances. *J Mater Chem*. 2010;20(11):2056. doi:[10.1039/b920406](#)
- Jin L, Nairn KM, Forsyth CM, Seeber AJ, MacFarlane DR, Howlett PC, Forsyth M, Pringle JM. Structure and Transport Properties of a Plastic Crystal Ion Conductor: Diethyl(Methyl)(Isobutyl)Phosphonium Hexafluorophosphate. *J Am Chem Soc*. 2012;134(23):9688–9697. doi:[10.1021/ja301175v](#)
- Uvarov NF, Asanbaeva NB, Ulihin AS, Mateyshina YG, Gerasimov KB. Thermal Properties and Ionic Conductivity of Tetra-n-Butylammonium Perchlorate. *Cryst*. 2022; 12(4):515. doi:[10.3390/cryst12040515](#)
- Yunis R, W. Newbegin T, F. Hollenkamp A, M. Pringle J. Ionic Liquids and Plastic Crystals with a Symmetrical Pyrrolidinium Cation. *Mater Chem Front*. 2018;2(6):1207–1214. doi:[10.1039/C8QM00016F](#)
- Guseva AF, Pestereva NN, Kuznetsov DK, Boyarshinova AA, Gardt VA. Conductivity of Composites MeWO<sub>4</sub>-Al<sub>2</sub>O<sub>3</sub> (Me = Ca, Sr). *Russ J Electrochem*. 2023;59(4):284–290. doi:[10.1134/S1023193523040079](#)

23. Uvarov NF, Hairetdinov EF, Skobelev IV. Composite Solid Electrolytes MeNO<sub>3</sub>-Al<sub>2</sub>O<sub>3</sub> (Me = Li, Na, K). *Solid State Ion.* 1996;86-88:577-580. doi:[10.1016/0167-2738\(96\)00208-1](https://doi.org/10.1016/0167-2738(96)00208-1)
24. Kubataev ZYu, Gafurov MM, Rabadanov KSh, Amirov AM, Akhmedov MA, Kakagasanov MG. The Effect of the Nanosized Oxide Filler on the Structure and Conductivity of Composite (1-x)(LiClO<sub>4</sub>-NaClO<sub>4</sub>)-xAl<sub>2</sub>O<sub>3</sub>. *Russ J Electrochem.* 2023;59(8):598-603. doi:[10.1134/S1023193523080050](https://doi.org/10.1134/S1023193523080050)
25. Ponomareva VG, Lavrova GV, Simonova LG. Effect of SiO<sub>2</sub> Morphology and Pores Size on the Proton Nanocomposite Electrolytes Properties. *Solid State Ion.* 1999;119(1-4):295-299. doi:[10.1016/S0167-2738\(98\)00517-7](https://doi.org/10.1016/S0167-2738(98)00517-7)
26. Ulihin AS, Uvarov NF. Electrochemical Properties of Composition Solid Electrolytes LiClO<sub>4</sub>-MgO. *Russ J Electrochem.* 2009;45(6):707-710. doi:[10.1134/S1023193509060135](https://doi.org/10.1134/S1023193509060135)
27. Uvarov NF, Ulihin AS, Slobodyuk AB, Kavun VY, Kirik SD. Nanocomposite Solid Electrolytes Based on Lithium Perchlorate. *ECS Trans.* 2008;11(31):9-17. doi:[10.1149/1.2953501](https://doi.org/10.1149/1.2953501)
28. Mateyshina Y, Uvarov N. The Effect of Oxide Additives on the Transport Properties of Cesium Nitrite. *Solid State Ion.* 2018;324:1-6. doi:[10.1016/j.ssi.2018.05.017](https://doi.org/10.1016/j.ssi.2018.05.017)
29. Ulihin AS, Uvarov NF, Rabadanov KSh, Gafurov MM, Gerasimov KB. Thermal, Structural and Transport Properties of Composite Solid Electrolytes (1-x)(C<sub>4</sub>H<sub>9</sub>)<sub>4</sub>NBF<sub>4</sub>-xAl<sub>2</sub>O<sub>3</sub>. *Solid State Ion.* 2022;378:115889. doi:[10.1016/j.ssi.2022.115889](https://doi.org/10.1016/j.ssi.2022.115889)
30. Adebahr J, Ciccossillo N, Shekibi Y, Macfarlane D, Hill A, Forsyth M. The "Filler-Effect" in Organic Ionic Plastic Crystals: Enhanced Conductivity by the Addition of Nano-Sized TiO<sub>2</sub>. *Solid State Ion.* 2006;177(9-10):827-831. doi:[10.1016/j.ssi.2006.02.022](https://doi.org/10.1016/j.ssi.2006.02.022)
31. Pringle JM, Shekibi Y, MacFarlane DR, Forsyth M. The Influence of Different Nanoparticles on a Range of Organic Ionic Plastic Crystals. *Electrochim Acta.* 2010;55(28):8847-8854. doi:[10.1016/j.electacta.2010.08.027](https://doi.org/10.1016/j.electacta.2010.08.027)
32. Mateyshina Y, Stebnitskii I, Shiltsov D, Ilyina E, Ulihin A, Bukhtiyarov A, Uvarov N. Hybrid Nanocomposite Solid Electrolytes (n-C<sub>4</sub>H<sub>9</sub>)<sub>4</sub>NBF<sub>4</sub>-MgO. *Int J Mo Sci.* 2023;24(13):10949. doi:[10.3390/ijms241310949](https://doi.org/10.3390/ijms241310949)
33. Mateyshina Y, Stebnitskii I, Uvarov N. Composite Solid Electrolytes (n-C<sub>4</sub>H<sub>9</sub>)<sub>4</sub>NBF<sub>4</sub>-Nanodiamonds. *Solid State Ion.* 2024;404:116419. doi:[10.1016/j.ssi.2023.116419](https://doi.org/10.1016/j.ssi.2023.116419)
34. Uvarov NF, Boldyrev VV. Size Effects in Chemistry of Heterogeneous Systems. *Russ Chem Rev.* 2001;70(4):265-284. doi:[10.1070/RC2001v070n04ABEH000638](https://doi.org/10.1070/RC2001v070n04ABEH000638)
35. Uvarov NF, Vaněk P, Yuzyuk YuI, Železný V, Studnička V, Bokhonov BB, Dulepov VE, Petzelt J. Properties of Rubidium Nitrate in Ion-Conducting RbNO<sub>3</sub>-Al<sub>2</sub>O<sub>3</sub> Nanocomposites. *Solid State Ion.* 1996;90(1):201-207. doi:[10.1016/S0167-2738\(96\)00400-6](https://doi.org/10.1016/S0167-2738(96)00400-6)
36. Stebnitsky IA, Uvarov NF, Mateyshina YuG. Synthesis and Study of the Physicochemical Properties of Composite Solid Electrolytes (C<sub>4</sub>H<sub>9</sub>)<sub>3</sub>CH<sub>3</sub>NBF<sub>4</sub>-Cnanodiamonds. *Russ J Electrochem.* 2024;60(1):18-24. doi:[10.1134/S1023193524010105](https://doi.org/10.1134/S1023193524010105)
37. Rabadanov KSh, Gafurov MM, Uvarov NF, Ulihin AS. Temperature-Phase Dependence of the Vibration Spectrum and Orientation Mobility of the Tetrafluoroborate Ion in n-Bu<sub>4</sub>NBF<sub>4</sub> Organic Salt. *Phys Solid State.* 2018;60(12):2593-2597. doi:[10.1134/S1063783418120235](https://doi.org/10.1134/S1063783418120235)
38. Uvarov NF. Composite Solid Electrolytes: Recent Advances and Design Strategies. *J Solid State Electrochem.* 2011;15(2):367-389. doi:[10.1007/s10008-008-0739-4](https://doi.org/10.1007/s10008-008-0739-4)